# Fast and Accurate Reconstruction of Compressed Color Light Field

# Ofir Nabati, David Mendelovic and Raja Giryes Tel Aviv University, Tel Aviv 6997801

ofirnabati@mail.tau.ac.il, mend@eng.tau.ac.il, raja@tauex.tau.ac.il

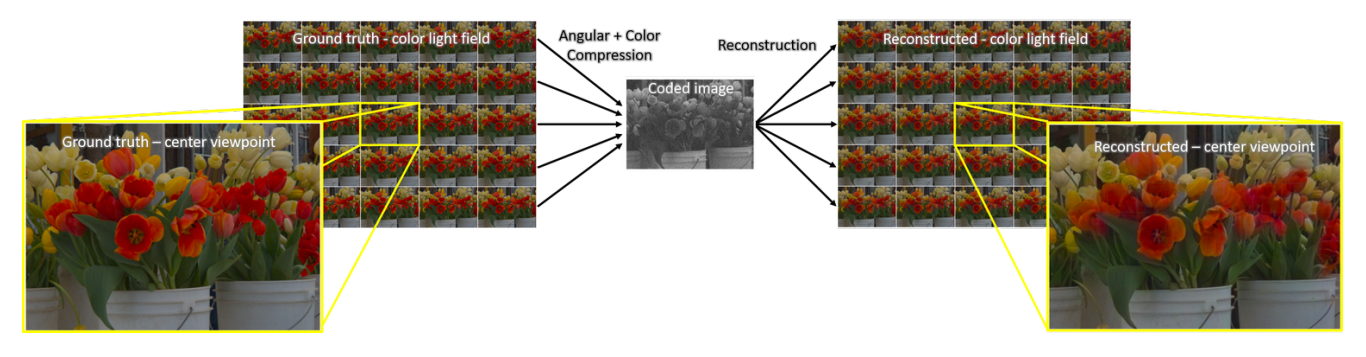


Figure 1: Reconstruction of a color light field image from a 2D coded image projected at the sensor in a single shot. The compression of the color and angular information is made by the optical system, using a random coded color mask between the aperture and the sensor. We reconstruct the color light field by using a neural network with a small computational time.

#### **Abstract**

Light field photography has been studied thoroughly in recent years. One of its drawbacks is the need for multilens in the imaging. To compensate that, compressed light field photography has been proposed to tackle the tradeoffs between the spatial and angular resolutions. It obtains using only one lens, a compressed version of the regular multi-lens system. The acquisition system consists of a dedicated hardware followed by a decompression algorithm, which usually suffers from high computational time. In our work, we suggest to compress the color channels as well and propose a computationally efficient neural network that achieves high-quality color light field reconstruction from a single coded image. Our approach outperforms existing solutions in terms of recovery quality and computational complexity. We also present a neural network for depth map extraction from the decompressed light field, which is trained in an unsupervised way without the ground truth depth map.

### 1. Introduction

While conventional 2D images contain only the RGB content of a given scene, light field images hold also its angular information. This allows performing several tasks

such as refocusing and depth extraction, which is harder to be done using only the spatial information. One way of representing light field information is as a collection of 2D images, taken from multi-viewpoints [26].

Light fields can be captured using various methods such as coded masks, coded apertures, microlenses and pinhole arrays. Due to limited sensor size, these systems suffer from a trade-off between the spatial and angular resolution that usually results in a sparse number of viewpoints. To address this drawback, bulky imaging systems or array of sensors [42] have been proposed. These solutions are either impractical or expensive as they require a large amount of storage and have a bigger size.

Recently, Marwah et al. have introduced the concept of **compressive light field photography** [30]. Relying on compressed sensing theory [7, 10], they reconstruct a high-resolution light field from its 2D coded projection measured by a single sensor. This theory guarantees under some conditions the recovery of a signal from a relatively small number of its linear measurements if the signal has a sparse representation in a given dictionary. In their case, a learned dictionary built from light field atoms has been used. Following this work, several improvements have been proposed for both the sensing system and the recovery algorithms [8, 15, 17]. Nevertheless, these methods still do not lead to real-time light field acquisition. Also, to the best of our

knowledge, there is no reference to **color** compression in these works.

Based on the strategy of Marwah et al., we propose a novel system for reconstructing color light fields from their compressed measurements acquired by a conventional camera with a random color mask. The light field estimation is performed by using deep learning, which is an emerging machine learning methodology that solves a given problem by training a neural network using a set of training examples. It achieves state-of-the-art results in various computer vision and image processing tasks such as image classification [23, 39], semantic segmentation [27], image denoising [35], image super-resolution [25], depth estimation [12], etc. Neural networks have been also implemented to synthesize new light field views from few given perspectives [21] or even a single view [37]. They have been used also to solve inverse problems with sparsity priors [14, 36] and specifically compressed sensing problems [2, 24]. These methods have shown to produce better and faster results than "classic" sparse coding techniques.

In this work, we use deep learning to reconstruct the compressed light field image. The coded color mask proposed in this work enables us to compress the color spectrum information of the light fields in a single shot. Our framework achieves state-of-the-art reconstruction quality with low computational time. Moreover, our network is designed to handle multiple types of mask patterns at the same time, allowing it to decompress light fields projected at various places on the sensor and by that, avoid the usage of multiple networks and excessive memory consumption, which is the practice in previous solutions [15].

The neural network in our work is a fully convolutional network (FCN) trained end-to-end using color 4D light field patches to solve the compressed sensing task. We compare our results on a light field dataset captured by a Lytro camera against dictionary-based approaches and another deep learning based method [15] demonstrating the superiority of the proposed strategy. Finally, we introduce an unsupervised-trained depth estimation network, which is concatenated with our light field reconstruction network, to extract depth maps directly from the compressed measurements. With less than a second in computation time, a usage of color compression and a memory efficient implementation, we believe that our work takes us one step closer to real-time high-resolution light field photography.

## 2. Related Work

#### 2.1. Capturing light field

Light field images have been recorded on a film sensor, using pinhole or microlens arrays, for over a century ago [19]. Light field information can be captured using multidevice systems (e.g. array of cameras [42]) or by time se-

quential imaging [26]. Both options are either clumsy and expensive or unsuitable for dynamic scenes. The lenslet-based approaches [1, 32] use microlens array, where each of them samples the angular distribution of the light field. Light field modulation techniques [40, 41] use coded masks or apertures, with patterns such as pinholes or sum of sinusoids, to multiplex the angular information into the sensor. All of the above methods sacrifice the spatial resolution of the sensor in favor of the angular resolution.

### 2.2. Compressed light field

Compressed light field allows reconstructing full resolution light field images from their coded projections. It has been first introduced by Marwah et al. [30]. In their work, a coded mask is placed between the sensor and the lenses to create a coded projection to the sensor. Then, the light field is reconstructed by sparse coding techniques such as OMP [33] or ISTA [5], in which, a learned dictionary of light field patches is used. Despite the fact that their solution allows high-resolution light field capturing, it suffers from huge computational complexity leading to hours of processing for a single light field scene.

Later works, regarding compressed light fields, have suggested alternative frameworks for the capturing and/or the reconstruction tasks: Hirsch et al. [17] introduced angle sensitive pixels (ASP), which create better conditions for recovery compared to mask-based approaches. They use the same time-consuming dictionary-based methods. Chen et al. [8] proposed a framework in which the disparity of the scene is first calculated by sub-apertures scan, followed by reconstruction using disparity-specific dictionary. While their framework achieved lower reconstruction time, it is still not enough for real-time usage as it takes few minutes. Moreover, their technique is limited to static scenes. It is important to mention that none of the above frameworks dealt with color compression.

### 2.3. Deep learning for light field reconstruction

Compressed sensing algorithms are usually computationally demanding, mainly because of their need for a significant amount of iterations. Gregor et al. [14] have addressed that problem by training an encoder network, with an architecture based on ISTA [5]. They have shown that their framework produces both better accuracy than ISTA and in much fewer iterations. Despite its benefits, LISTA is a fully connected network, which limits the patch size due to memory limitations and the large number of training examples required in the case of large patches. Therefore, an alternative neural network architecture is required.

Other neural network based solutions for compressed sensing has been already done for MRI reconstruction [29] and compressed CT [16]. Gupta et al. [15] have proposed such a method for compressed light fields. They trained a

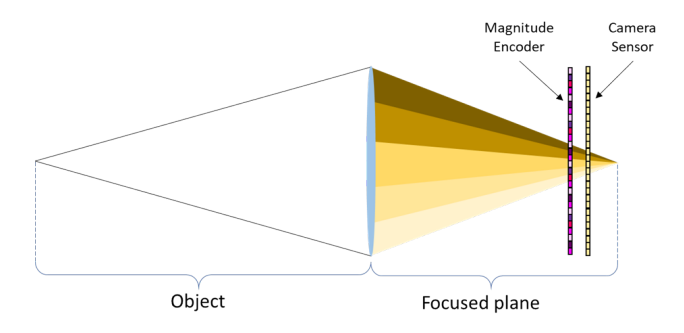


Figure 2: A scheme of the light field acquisition system with the color coded random mask. Different viewpoints are coded at different places at the coded mask. Thus, each angle has a different weight in  $\Phi$  for every color channel.

two-branch network to decompress compressed light fields for various sensing frameworks. One of those branches is a fully connected network, which like LISTA, limits the patch size. Also, their network architecture is adjusted for only one mask pattern and therefore, it is not invariant to different locations on the sensor as each patch on the sensor is generated by a different compressing matrix. Srinivasan et al. [37] have used dilation networks in order to synthesize new viewpoints from only the center view in addition to the depth map of the scene. While they succeed to do so for specific scenes, their system rely on a large aperture camera and is limited to the class of images it was trained on.

## 3. Color light field capturing

In this section we provide details on the color 4D light field images and their coded projections. In addition, we describes our compressed sensing problem and the properties of our color coded mask [31].

### 3.1. Mathematical background

Following the plenoptic multiplexing approach in [41] and the representation of light fields in [32], we define the contiguous color light field as  $l_{\lambda}(\mathbf{x},\mathbf{v}) = l(\mathbf{x},\mathbf{v},\lambda)$ , which denotes the ray that intersects the aperture plane at  $\mathbf{x}$  and the sensor plane at  $\mathbf{v}$  over the color spectrum  $\lambda$ . A point at the sensor image is an integration over the aperture of all light rays that reach this point, over all the spectrum, coded by the mask between the sensor and the aperture:

$$i(\mathbf{x}) = \iint l(\mathbf{x}, \mathbf{v}, \lambda) M(\mathbf{x}, \mathbf{v}, \lambda) \cos^4 \theta \, d\mathbf{v} \, d\lambda, \quad (1)$$

where  $M(\mathbf{x}, \mathbf{v}, \lambda)$  is the modulation function characterized by the coded mask and  $\theta$  is the angle between the ray  $(\mathbf{x}, \mathbf{v})$  and the sensor plane. The  $\cos^4 \theta$  factor represents the vi-

gnetting effect [34]. To simplify the equation, we denote:

$$\tilde{M}(\mathbf{x}, \mathbf{v}, \lambda) = M(\mathbf{x}, \mathbf{v}, \lambda) \cos^4 \theta.$$
 (2)

Thus, for a specific color spectrum we get

$$i_{\lambda}(\mathbf{x}) = \int l_{\lambda}(\mathbf{x}, \mathbf{v}) \tilde{M}(\mathbf{x}, \mathbf{v}, \lambda) \, d\mathbf{v}. \tag{3}$$

For discrete light fields, we have a vectorized version of (3). For each color channel, taking the noise into account, we have

$$\mathbf{i}_{\lambda} = \mathbf{\Phi}_{\lambda} \mathbf{l}_{\lambda} + \mathbf{n}, \ \mathbf{\Phi}_{\lambda} = [\mathbf{\Phi}_{\lambda,1} \ \mathbf{\Phi}_{\lambda,2} \ \cdots \ \mathbf{\Phi}_{\lambda,N_{\sigma}^{2}}],$$
 (4)

where  $\mathbf{i}_{\lambda} \in \mathbb{R}^m$  is the vectorized sensor image,  $\mathbf{l}_{\lambda} \in \mathbb{R}^k$  is the vectorized light field, and  $\Phi_{\lambda,i} \in \mathbb{R}^{m \times m}$  is the modulation matrix of the ith viewpoint over the spectrum  $\lambda$ .  $\Phi_{\lambda} \in \mathbb{R}^{m \times k}$  is a concatenation of  $\Phi_{\lambda,i}$ , i.e., it is the sensing matrix based on the modulation of the projected light field at the sensor.  $N_v$  is the angular resolution of the light field for a single axis. Thus, the discrete light field has  $N_v^2$  different viewpoints. Also, if the spatial resolution of the light field is  $N_x \times N_x$  then  $m = N_x^2$  and  $k = N_x^2 \cdot N_v^2$ .  $\mathbf{n} \in \mathbb{R}^m$  is an i.i.d zero mean Gaussian noise with variance  $\sigma^2$ .

The discrete color spectrum is the RGB color space  $\lambda \in \{\lambda_R, \lambda_G, \lambda_B\}$ . Hence, we can generalize (4) to a color light field :

$$\mathbf{i} = [\mathbf{\Phi}_{\lambda_B} \; \mathbf{\Phi}_{\lambda_G} \; \mathbf{\Phi}_{\lambda_B}] \mathbf{l} + \mathbf{n} = \mathbf{\Phi} \mathbf{l} + \mathbf{n}, \tag{5}$$

where  $\mathbf{l}=[\mathbf{l}_{\lambda_R}\ \mathbf{l}_{\lambda_G}\ \mathbf{l}_{\lambda_B}]^T$  and now  $k=N_x^2\cdot N_v^2\cdot 3$  for RGB color channels. While (4) is the sum of each discrete viewpoint, coded by its appropriate sensing matrix  $\Phi_{\lambda,i}$ , in (5) we have also the summation over the 3 color channels. The compression ratio of the system is  $\frac{m}{k}=\frac{1}{N_v^2\cdot 3}$ , which means that for  $N_v^2=25$  viewpoints, the compression ratio is 1.3%. Also, the overall light which reaches the sensor is divided between each sub-aperture image among each of its color channels. Therefore, every color channel of sub-aperture image is attenuated by the same compression ratio, so the effective  $\Phi$  matrix is:  $\Phi=\frac{1}{N_v^2\cdot 3}\tilde{\Phi}$ , When  $\tilde{\Phi}$  is the unattenuated matrix. Due to this phenomena, the reconstruction process has higher noise sensitivety as the compression ratio increase.

From compressed sensing perspective, the inverse problem that we wish to solve is:

$$\underset{\boldsymbol{\alpha}}{\operatorname{argmin}} \|\boldsymbol{\alpha}\|_{0} \ s.t \ \|\mathbf{i} - \boldsymbol{\Phi} \mathbf{D} \boldsymbol{\alpha}\|_{2}^{2} < \epsilon, \tag{6}$$

where  $\|\cdot\|_0$  is the  $l_0$  pseudo-norm,  $\epsilon = \|\mathbf{n}\|_2^2$ ,  $\mathbf{D} \in \mathbb{R}^{k \times s}$  is a given transform matrix or a learned dictionary and  $\alpha \in \mathbb{R}^s$  is the sparse representation of the light field  $\mathbf{l}$ . This problem is a NP-hard problem. It can be solved using a greedy algorithm such as OMP [33] or by relaxation to a  $\ell_1$  minimization problem, which is also known as basis pursuit denoising (BPDN) or LASSO, and has many solvers (e.g. [5, 6]).

Due to physical constraints,  $\Phi_{\lambda,i}$  are diagonal matrices and  $\Phi$  is a concatenation of them (see Fig. 3 top). Therefore,  $\Phi \mathbf{D}$  has high mutual coherency [11] and has no theoretical guarantee for successful reconstruction. However, empirical evidence has shown that the light field images can be restored, even without these guarantees.

## 3.2. The color mask

In order to multiplex the color information of the intersected rays into the projected 2D image at the sensor, we use a color mask, which unlike bayer CFA pattern [4], is random. The position of the mask should also enable us to multiplex the angular information of the rays. Therefore, the mask should not be placed directly on the sensor but slightly further, as mentioned in [30]. This position, in addition to the color pattern, allows having random weights for different angles and colors. It is important to mention that the effective weights of  $\Phi$  cannot be taken directly from the color mask, but by an accurate ray tracing computation over all the possible  $\mathbf{x}, \mathbf{v}$  and the three color channels. Therefore, the relationship between the mask and  $\Phi$  is not direct.

A simpler approach to calculate  $\Phi$  is to illuminate the sensor from each viewpoint, using white LED and three color filters. Then,  $\Phi_{\lambda,i}$  can be easily taken from the pattern projected at the sensor. Yet, for simplicity, in our simulation we assume  $\Phi$  to be as the mask. To make it as realistic as possible, we will not assume periodic mask or any specific structure of it as done in previous work [15, 30], because as mentioned above, periodicity in the mask does not imply periodicity in  $\Phi$ . Instead, we assume a random mask that implies that  $\Phi$  is also random, which is more realistic. From now on,  $\Phi$  will be a tensor of the size  $N_x \times N_x \times N_v \times N_v \times 3$  (see Fig 3 bottom), where each index corresponds to the weight modulation of a specific ray  $(\mathbf{x}, \mathbf{v}, \lambda)$ .

## 4. Light Field Reconstruction Network

In our work, we use a FCN which enables processing of large patches (we use a size of 100x100). To make the network robust to the location of the patch in the image, it gets as an input also the the corresponding part in  $\Phi$ . This allows training a single network for the whole light field scene. We turn to describe now the network design, which allows fast reconstruction. In Section 6, we compare our network results against dictionary based methods along with another deep learning method.

The network receives as input the compressed image and its matching sensing tensor:

$$\hat{\mathbf{l}} = f(\mathbf{i}, \mathbf{\Phi}),\tag{7}$$

where  $\hat{\mathbf{l}}$  is the reconstructed light field patch, and  $\mathbf{i}$  and  $\boldsymbol{\Phi}$  are the compressed patch and its matching sensing tensor of

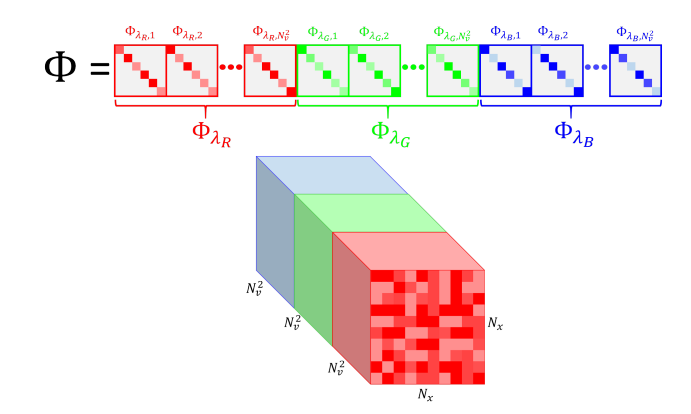


Figure 3: (**Top**)  $\Phi$  **matrix:** Because of physical constraints, the sensing matrix for each viewpoint and color channel is a diagonal matrix.  $\Phi \in \mathbb{R}^{N_x^2 \times N_x^2 \cdot N_x^2 \cdot 3}$  is a concatenation of these matrices over all viewpoints and color channels. (**Bottom**)  $\Phi$  **tensor:**  $\Phi$  can be also expressed as a 5-D tensor. Each element in it is the modulation weight for a specific ray  $(\mathbf{x}, \mathbf{v}, \lambda)$ . In the above figure, we present a tensor  $\Phi$  in which the angular dimensions and the color dimension are concatenated together. This is the tensor  $\Phi$  we use as part of the input to our reconstructed network (see Fig. 4).

corresponding location at the sensor. Due to memory limitations, our network does not process the whole image at once but in a patch based manner. In order to avoid block artifacts, we reconstruct the patches with an overlap between them according to a predefined stride size. We have observed that the peripherally pixels of each patch are usually restored with less accuracy compared to the inner pixels. Therefore, we average the patches using Gaussian weights:

$$\hat{l}(\mathbf{x}, \mathbf{v}, \lambda) = \frac{\sum_{\mathbf{x}_0 \in \mathbf{X}} P_{\mathbf{x}_0} G_{\sigma}(\mathbf{x} - \mathbf{x}_0, \mathbf{v}, \lambda)}{\sum_{\mathbf{x}_0 \in \mathbf{X}} G_{\sigma}(\mathbf{x} - \mathbf{x}_0, \mathbf{v}, \lambda)},$$
(8)

where  $P_{\mathbf{x}}$  is the recovered patch whose center is at  $\mathbf{x}$ .  $G_{\sigma}(\mathbf{x}, \mathbf{v}, \lambda)$  is a zero mean 2D isotropic Gaussian with variance  $\sigma$  and the same support as  $P_{\mathbf{x}}$ .

#### 4.1. Network architecture

Due to their success in various tasks, we chose convolutional neural network as our regression model for the reconstruction. Convolutional networks allow us to process large patches with a low computational time. Our network architecture is a dilated convolutional network [43]. Dilated convolutions enables the expansion of the receptive fields of the network using a small filter size, without performing any pooling or sampling. This enables us to keep the original resolution of the network without making the network too deep, which may harm the computation time and lead

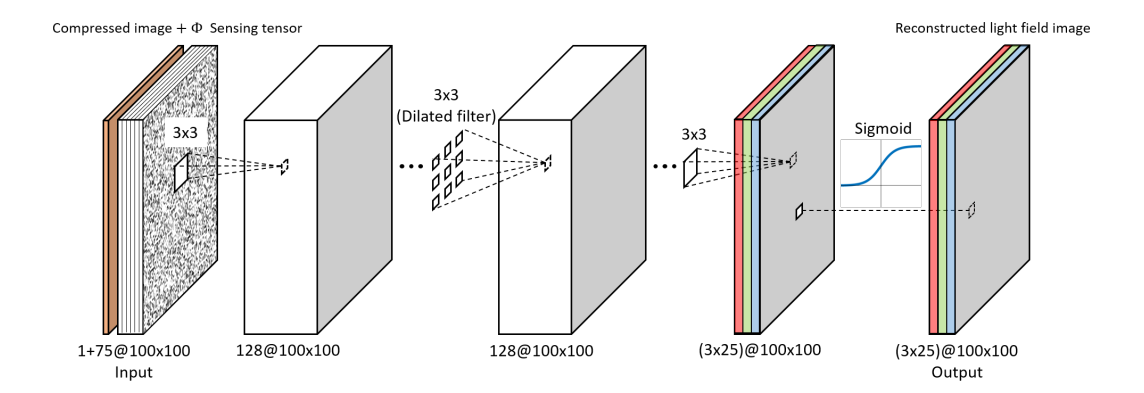


Figure 4: Our reconstruction network consists of  $11.3 \times 3$  convolutional layers with 128 channels. The middle four layers are dilated convolutional layers. All the layers, except of the last one, are followed by a batch normalization and ELU. The last layer is followed by a sigmoid enforcing the output range to [0, 1]. The network input is a concatenation of the compressed image and the sensing tensor (see Fig 3). The output is the decompressed color light field image, which consists of 5x5 viewpoints across 3 color channels (thus, we have 3x25 channels in the last two layers).

to over-fitting. This type of network was originally created for semantic segmentation but appears to be also suitable for our compressed sensing reconstruction task as well.

Each convolution layer in our network is followed by an exponential linear unit (ELU) [9] and batch normalization [18], except at the last layer, where a sigmoid is used in order to force the output to be in the range [0,1]. All filters are of size  $3\times 3$  without any exception. The dilations used in the network are with exponentially increasing rates as mentioned in [43]. We found that big patches leads to better reconstruction. Therefore, our network reconstructs patches with size  $100\times 100\times 5\times 5\times 3$  (the  $5\times 5\times 3$  stands for the number of reconstructed angles and the color channels).

The network has 11 convolution layers of which the middle four are dilated convolutional layers with exponentially increasing rates of 2-4-8-16. All layers have 128 channels. We chose a stride of half patch size for the patch averaging, which results in a good trade off between reconstruction quality and computational time. The simulated mask was randomly generated as a RGBW color mask, which means every pixel is either red,green,blue or white (all colors pass).

#### 4.2. Robustness for the sensing matrix

The input to the network is the compressed color light field patch, concatenated with its matching  $\Phi$  tensor. Adding  $\Phi$  to the input improves the reconstruction, but more importantly, it allows the network to be adaptive to different types of  $\Phi$ . In fact, this important property makes the network useful for compressed patches from different places at the sensor, which correspond to different sensing matrices. Therefore, this allows us to train **only one** network for the whole sensor, which leads to a very small memory usage and computational time compared to the

case where a different network is used for each patch.

## 4.3. Training

We mark the set of light field patches from our training images as  $\mathcal{T}$ . We also create a dataset of different  $\Phi$  tensors which correspond to all the locations on the sensor that we use during recovery (which are set according to a wanted stride size). We mark this data set as  $\mathcal{M}$ . For each batch of size B, we randomly choose light field patches from  $\mathcal{T}$  and sensing tensors from  $\mathcal{M}$ . Then we create their matching compressed patches  $\{\mathbf{i}_q\}_{q=1}^B$ :

$$\mathbf{i}_q = \mathbf{\Phi}_q(\mathbf{l}_q) + \mathbf{n}, \ \mathbf{l}_q \in \mathcal{T}, \ \mathbf{\Phi}_q \in \mathcal{M},$$
 (9)

where the training set is the group of tuples  $\{(\mathbf{i}_q, \mathbf{\Phi}_q, \mathbf{l}_q)\}_{q=1}^B$ , in which every tuple consists of the ground truth light field patch  $\mathbf{l}_q$ , its corresponding sensing tensor  $\mathbf{\Phi}_q$  and its compressed measurement  $\mathbf{i}_q$ .  $\mathbf{n}$  is the model's sensor noise  $\mathbf{n} \sim \mathcal{N}(0, \sigma_{sensor}^2)$ . This way we create combinations of various light field patches with randomly chosen locations in our sensing tensor.

The network training loss function consists of two parts:

$$\mathcal{L} = \sum_{q} \underbrace{\|\hat{\mathbf{l}}_{q} - \mathbf{l}_{q}\|_{1}}_{\mathcal{L}_{data}} + \beta \underbrace{\|\mathbf{\Phi}_{q}(\hat{\mathbf{l}}_{q}) - \mathbf{i}_{q}\|_{2}^{2}}_{\mathcal{L}_{cs}}, \tag{10}$$

where  $\beta$  is a hyper parameter balancing  $\mathcal{L}_{data}$  and  $\mathcal{L}_{cs}$ . The data term  $\mathcal{L}_{data}$  is the  $\ell_1$  distance between the reconstructed light field patch and the ground-truth patch. We have chosen the  $\ell_1$  norm because it has shown to be more robust to noise compared to the  $\ell_2$  distance [45]. The second term  $\mathcal{L}_{cs}$  imposes consistency with the measurements model. Once the network training converges, we fine tune the network using the  $\ell_2$  distance in  $\mathcal{L}_{data}$  instead of the  $\ell_1$  norm. This action improves the recovery accuracy by 0.5 PSNR.

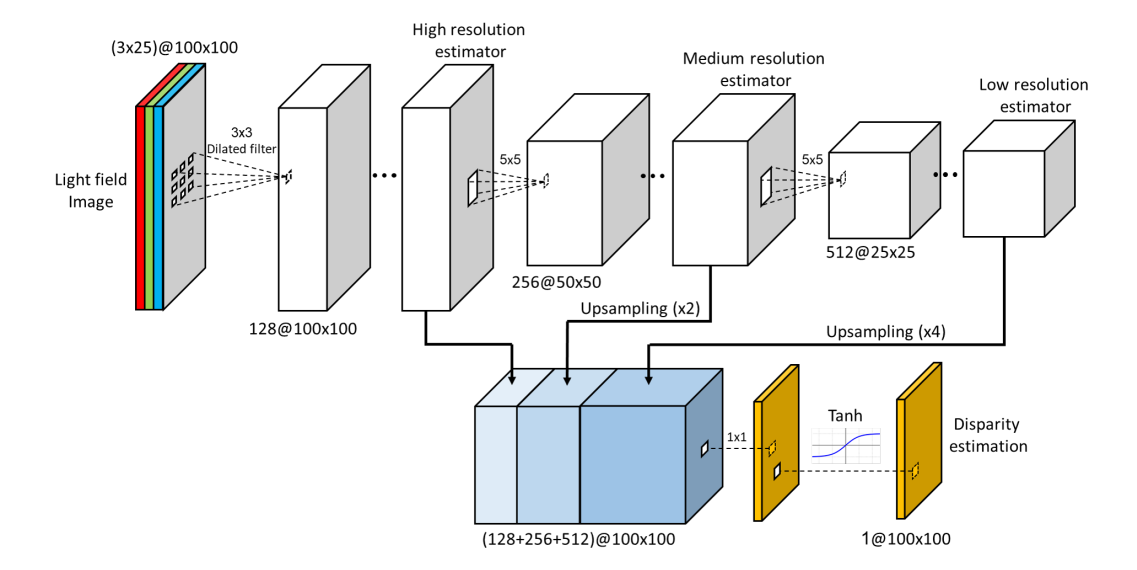


Figure 5: Our disparity network consists of a dilated convolutional network followed by downsampling, convolutions, another downsampling and more convolutions. Downsampling is done by a 2-stride convolution. The outputs of all resolution levels are concatenated after upsampling the medium and low resolution maps using transposed convolutions. A 1x1 convolution is applied on the concatenated maps followed by a scaled tanh at the output that provides the estimated disparity field.

## 5. Disparity Map Network

In [37], a dilated convolutional network is proposed, as part of the light field extraction framework, in order to extract a disparity map of the input. We use a modified version of their network and loss function. Our network reconstructs the depth map from the light field image instead of the center view as done in [37]. Also, the output is a single disparity field that maps the viewpoints to the center view and not a disparity map for each angle as done in their work.

The first 7 layers in our network consist of dilated convolutions with 128 channels and rates of 1-1-2-4-8-16-16 in order to create a prediction of the disparity map in full resolution. Then, we perform down sampling by using convolutions with stride 2, apply 3 additional convolutions with 256 channels, and then down sample again. We end by other 3 more convolutional layers with 512 channels. This way, we create two more disparity predictions with lower spatial resolution but with greater disparity reliability.

Every layer is followed by an ELU and batch normalization. At the end, we upsample these low resolution maps with transposed convolutional layers [44] and concatenate them along with the full resolution map using skip connections. This action is followed by a 1x1 convolution layer and tanh, which is scaled to the maximum allowed disparity. All filters are 3x3 except of the downsampling and upsampling layers, which are 5x5 filters and the last layer of the network, which is 1x1 convolution. The network's input is a light field image and its output is the estimated disparity

map:

$$\mathbf{d} = g(\mathbf{l}). \tag{11}$$

The loss function is similar to [37] but with one crucial difference. Instead of rendering the center viewpoint to all other angels. We render all viewpoints to the center view using the disparity map at the output. This change reduce the redundancy of the disparity tensor and enforce more accurate estimation, which is based on every angle instead of just one. Due to the fact that we have only one disparity map, we do not need to use consistency regularization of the disparity map as in [37]. Our loss function is:

$$\mathcal{L}_{D} = \sum_{q} \frac{1}{N_{v}^{2}} \sum_{i=1}^{N_{v}^{2}} ||\tilde{\mathbf{l}}_{q}^{i} - \mathbf{l}_{q}^{c}||_{1} + \gamma \ell_{\text{TV}}(\mathbf{d}_{q}), \quad (12)$$

where q is the patch index at the training batch  $\{\mathbf{l}_q\}_{q=1}^B$ ,  $\tilde{\mathbf{l}}_q^i$  is the ith viewpoint rendered to the center view, using the estimated disparity field  $\mathbf{d}$ , and  $\mathbf{l}_q^c$  is the ground-truth center view. The rendered light field image is constructed by using the next connection (see more details in [37]):

$$\tilde{l}^{i}(\mathbf{x}, \lambda) = l(\mathbf{x} - \mathbf{k}d(\mathbf{x}), \mathbf{k}, \lambda). \tag{13}$$

This formula is due to the depth consistency of the same point across different viewpoints without considering occlusions or non-Lambertian effects.  $\mathbf{k}$  is the corresponding viewpoint position of the ith index out of the total  $N_v^2$  viewpoints. Notice that like [37], there is no usage of the ground



Figure 6: Reconstruction results on test images. Our network's reconstruction time takes less than 0.5 sec for the whole light field images. Note that our network's results are with high spatial quality and that in the noisy case they have lower color fidelity. We present also the reconstruction results for compressed light fields with  $\Phi$  that was never been observed in training. This demonstrates the robustness of the proposed approach.

truth depth map. This network can be concatenated with the reconstruction network. Thus, a disparity map can be estimated directly from the compressed image:  $\mathbf{d} = g(f(\mathbf{i}, \Phi))$ .

## 6. Experiments

We present our results for color light field decompression on the Stanford Lytro dataset [38] and the Lytro dataset provided by Kalantari et al. [21]. In addition, we show our reconstructed disparity maps from the compressed image. All of our networks have been trained in tensorflow using color patches of size  $100 \times 100$  with an angular resolution of  $5 \times 5$  (25 viewpoints). The training has been done with mini-batches of size 32, the filters have been initialized using Xavier initialization [13], and the ADAM optimizer [22] has been used with  $\beta_1=0.9, \beta_2=0.999$  and an exponentially decaying learning rate. The dataset includes 79 light fields images of size  $376 \times 541 \times 5 \times 5 \times 3$ , which means that there are over 9 millions  $100 \times 100$  patches in it, which are different by at least a single pixel from each other. We have chosen 7 light field images as the test set while the rest have been kept for training.

For the reconstruction network, we set  $\beta$ =0.004 and the initial learning rate to 0.0005. For the patch averaging,  $\sigma$  is set to 1. For the disparity network, we set  $\gamma=0.1$  in (12) and the initial learning rate to 0.001.  $\sigma$  is set to 0.2.

#### 6.1. Light field reconstruction evaluation

We evaluated two scenarios. One with clean observations and the second with noisy ones with  $\sigma_{sensor}=0.02$ . We present the average PSNR and SSIM across our 7 test light field images. Both networks were trained with 800 epochs, each includes randomly chosen 4000 patches.  $\Phi$  was randomly chosen without any optimization as we de-

scribe in section 3.2. The reconstructed light field patches were restored with their matching  $\Phi$  tensors using only one network for the whole image. We compare our results with dictionary-based methods. The dictionary was trained on color light field 8x8 patches. It was trained using online dictionary learning [28] in order to overcome memory limits, which was initialized using K-SVD [3] trained on a smaller dataset. The reconstruction was made with OMP [33] and ADMM [6] with patch overlapping of 2 pixels, using Intel i7-6950X CPU with 10 cores. Our network used NVIDIA GeForce GTX 1080 Ti both for training and testing.

Figure 6 presents the quality of our reconstruction for two light field images out of our test set. Note the high accuracy in the reconstruction of the various details in the image. Yet, in the noisy case, we suffer from lower color fidelity because of the high compression ratio. Nevertheless, in this case, the reconstructed images have high spatial quality. To check the ability of our network to generalize to new compression patterns of  $\Phi$ , we have tested the network with an entirely new randomly generated  $\Phi$ , whose patterns have never been observed by the network in training time. Our results show that switching to the new  $\Phi$  has not affected the results at all. This approves that our network generalizes well to new compression patterns.

Figure 7 makes a comparison between our network and sparsity-based methods (OMP and ADMM) for other two light field images from the test set. At the noiseless example (bottom), our reconstruction has the highest color fidelity and spatial quality, while the other methods suffer from artifacts and low saturation of the colors. In the noisy case (top), OMP fails to recover the details and colors of the image almost completely while losing all the angular resolution (shown in Appendix A). Also, ADMM suffers from noisy reconstruction while our network's output

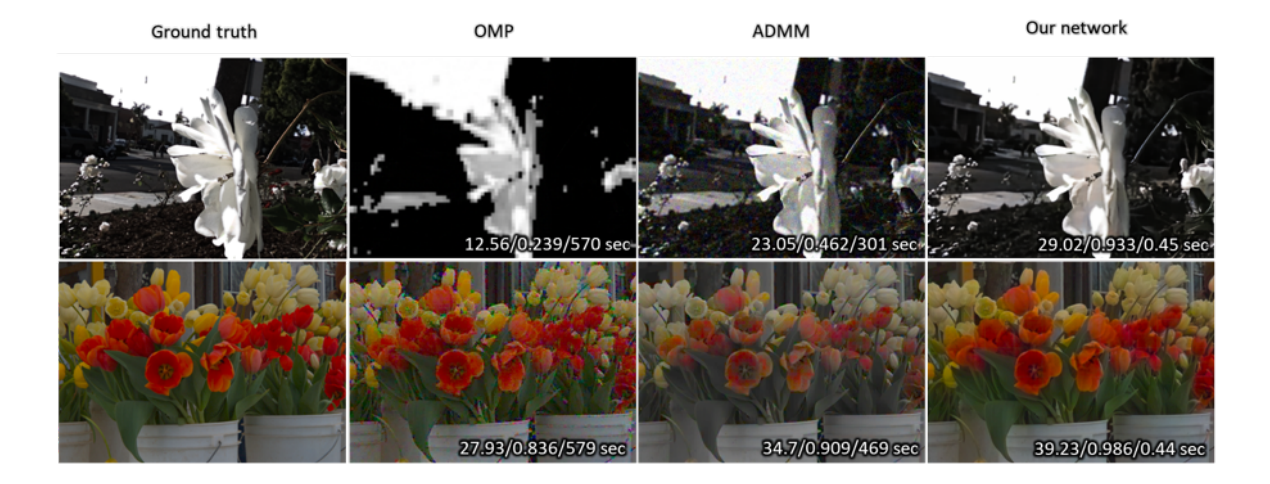


Figure 7: Comparison between our reconstruction network and dictionary-based methods. The presented numbers are PSNR/SSIM/reconstruction time. **Top:** noisy case with  $\sigma_{sensor}=0.02$ . **Bottom:** Noiseless case. Note that our method is both faster and more accurate than the sparse coding based approaches.

is clean and has high reconstruction quality. On top of all that, our method takes 3 orders of magnitude less time than the sparsity methods.

Tables 1 and Table 2 summarize the average PSNR and SSIM both for the noisy and noiseless cases. In the noiseless case we also compare to Gupta et al. [15]. It can be clearly seen that our framework is superior in terms of reconstruction quality, computational time and has higher robustness to noise. The average reconstruction time of our network in both cases is **0.46 sec** for a single light field scene, which is faster by 1-2 orders of magnitude compared to other previous existing solutions. More light-field reconstruction examples are provided in Appendix A.

According to the reported results in [15], the reconstruction of noise-free images with their network on 3 reported images (Seahorse, Purple flower and White flower) has worse PSNR than ours on the same images and takes one order of magnitude more time compared to our reconstruction using Titan X GPU (reported results are in Table 1). Note that their network does not deal with color compression but decompress each channel separately. Therefore, our compression ratio is three times lower than theirs, which is harder to decompress. Also, their network is not robust to different types of  $\Phi$  but is adjusted to only one patch pattern, which means that they have to train a different network for each patch. Note that they use ASP [17], which creates a different  $\Phi$  compared to coded mask.

#### **6.2.** Disparity estimation evaluation

In order to evaluate our disparity network, we examine its depth estimation quality given the ground truth light field

	PSNR	SSIM	Reconst. time
Ours	32.16	0.97	0.46 sec
OMP	19.83	0.71	562 sec
ADMM	27.56	0.85	345 sec
Gupta et al. [15]	30.9*	-	80 sec

Table 1: Average results for noise-free model. We compare out results against dictionary-based methods and [15]. \*Average results of 3 images reported in [15] for the Lytro test set in noiseless case. In that work, the decompression is made for each color channel separately and compression is done with ASP.

	PSNR	SSIM	Reconst. time
Ours	28.9	0.93	0.46 sec
OMP	12.93	0.17	556 sec
ADMM	24.16	0.52	294 sec

Table 2: Average results in the noisy case. We compare our results against sparsity-based methods.

and also given the recovered light field of our reconstruction network. We compare our disparity maps to the disparity estimation of Jeon at el. [20], which is considered to be the state-of-the-art for disparity evaluation from light field images. Their method uses no learning and relies on graphcuts of a big cost volume.

Fig. 8 shows the recovery of each method. Our net-

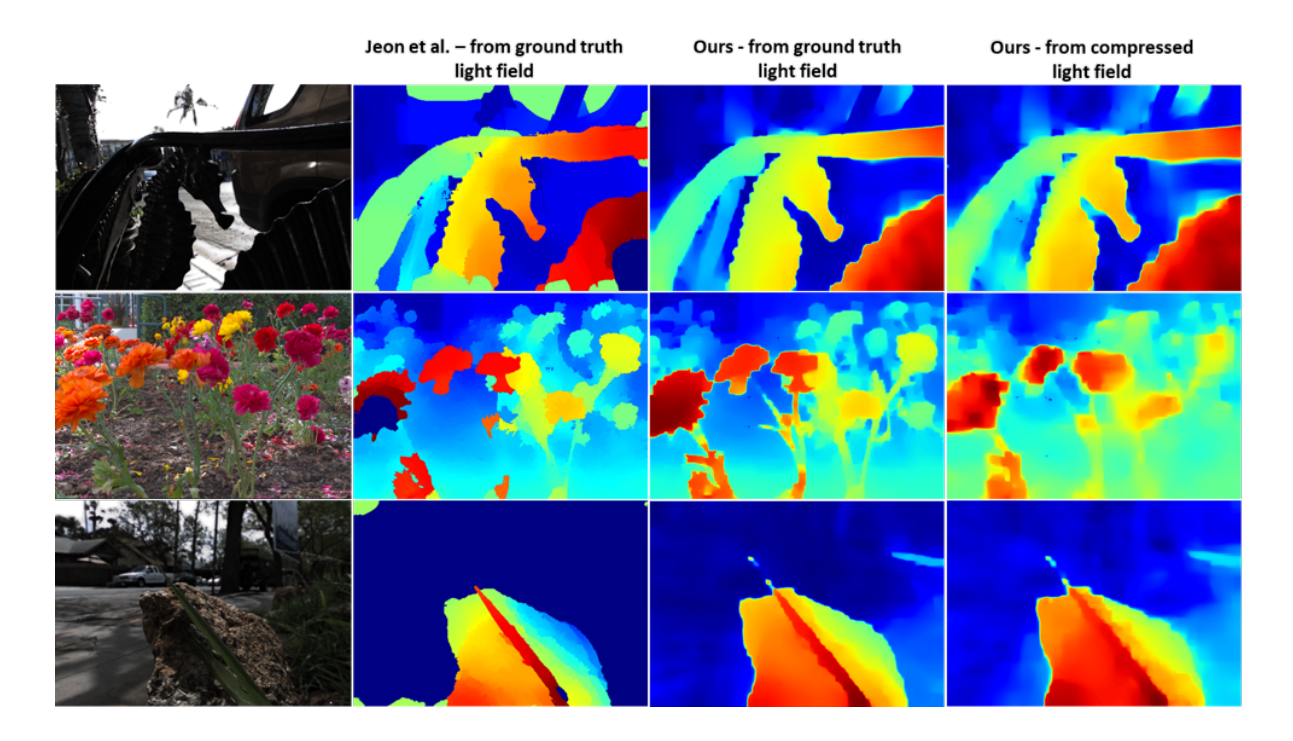


Figure 8: Comparison of disparity estimation. Warmer colors indicate greater disparity. We present here disparity maps that were calculated from the ground truth light field image and also from the reconstructed image. We compare our results to Jeon et al. [20], which is considered to be the state-of-the-art at depth estimation from light field images. Their algorithm is demonstrated on the ground truth light field only. Note that our network produces more detailed and accurate disparity maps but with more background noise and blur compared to Jeon et al.

work succeeds to preserve more image details and structure. Moreover, it has less false predictions in the background pixels. Yet, it suffers from noisy background and blur in the disparity. More depth estimation examples are provided in Appendix B. In computation time, our network requires less than a second to calculate the disparity map using NVIDIA GeForce GTX 1080 Ti while Jeon et al. technique takes over 80 seconds using Intel i7-6950X CPU with 10 cores.

#### 7. Conclusions

A novel system for reconstructing color light fields from their compressed measurements coded with a random color mask has been proposed. The processing is performed by an efficient neural network that uses a small amount of memory, has low computational time and is robust to different compression patterns. We also have demonstrated how a reconstructed light field image can be used to estimate the depth of the scene using another neural network. We believe that this framework can be translated into a real compressed color light field camera, which is mobile, small and cheap.

#### 8. Acknowledgments

This research was supported by the Yitzhak and Chaya Weinstein Research Institute for Signal Processing.

#### References

- [1] E. H. Adelson and J. Y. Wang. Single lens stereo with a plenoptic camera. *IEEE transactions on pattern analysis and machine intelligence*, 14(2):99–106, 1992.
- [2] A. Adler, D. Boublil, and M. Zibulevsky. Block-based compressed sensing of images via deep learning. In *IEEE 19th International Workshop on Multimedia Signal Processing (MMSP)*, pages 1–6, Oct 2017.
- [3] M. Aharon, M. Elad, and A. Bruckstein. rmk-svd: An algorithm for designing overcomplete dictionaries for sparse representation. IEEE Transactions on signal processing, 54(11):4311–4322, 2006.
- [4] B. E. Bayer. Color imaging array, July 20 1976. US Patent 3,971,065.
- [5] A. Beck and M. Teboulle. A fast iterative shrinkage-thresholding algorithm for linear inverse problems. *SIAM journal on imaging sciences*, 2(1):183–202, 2009.
- [6] S. Boyd, N. Parikh, E. Chu, B. Peleato, and J. Eckstein. Distributed optimization and statistical learning via the al-

- ternating direction method of multipliers. *Foundations and Trends*(R) *in Machine Learning*, 3(1):1–122, 2011.
- [7] E. J. Candès and M. B. Wakin. An introduction to compressive sampling. *IEEE signal processing magazine*, 25(2):21–30, 2008.
- [8] J. Chen and L.-P. Chau. Light field compressed sensing over a disparity-aware dictionary. *IEEE Transactions on Circuits* and Systems for Video Technology, 27(4):855–865, 2017.
- [9] D.-A. Clevert, T. Unterthiner, and S. Hochreiter. Fast and accurate deep network learning by exponential linear units (elus). Proceedings of the International Conference on Learning Representations (ICLR), 2016.
- [10] D. L. Donoho. Compressed sensing. *IEEE Transactions on information theory*, 52(4):1289–1306, 2006.
- [11] D. L. Donoho, M. Elad, and V. N. Temlyakov. Stable recovery of sparse overcomplete representations in the presence of noise. *IEEE Transactions on information theory*, 52(1):6–18, 2006.
- [12] J. Flynn, I. Neulander, J. Philbin, and N. Snavely. Deepstereo: Learning to predict new views from the world's imagery. In *Proceedings of the IEEE Conference on Computer Vision and Pattern Recognition*, pages 5515–5524, 2016.
- [13] X. Glorot and Y. Bengio. Understanding the difficulty of training deep feedforward neural networks. In *Proceedings* of the Thirteenth International Conference on Artificial Intelligence and Statistics, pages 249–256, 2010.
- [14] K. Gregor and Y. LeCun. Learning fast approximations of sparse coding. In *Proceedings of the 27th International Con*ference on Machine Learning (ICML-10), pages 399–406, 2010.
- [15] M. Gupta, A. Jauhari, K. Kulkarni, S. Jayasuriya, A. Molnar, and P. Turaga. Compressive light field reconstructions using deep learning. In *Proceedings of the IEEE Conference on Computer Vision and Pattern Recognition Workshops*, pages 11–20, 2017.
- [16] Y. Han, J. Yoo, and J. C. Ye. Deep residual learning for compressed sensing ct reconstruction via persistent homology analysis. *arXiv preprint arXiv:1611.06391*, 2016.
- [17] M. Hirsch, S. Sivaramakrishnan, S. Jayasuriya, A. Wang, A. Molnar, R. Raskar, and G. Wetzstein. A switchable light field camera architecture with angle sensitive pixels and dictionary-based sparse coding. In *IEEE International Con*ference on Computational Photography (ICCP), pages 1–10, 2014
- [18] S. Ioffe and C. Szegedy. Batch normalization: Accelerating deep network training by reducing internal covariate shift. In *International Conference on Machine Learning*, pages 448– 456, 2015.
- [19] F. E. Ives. Parallax stereogram and process of making same., Apr. 14 1903. US Patent 725,567.
- [20] H.-G. Jeon, J. Park, G. Choe, J. Park, Y. Bok, Y.-W. Tai, and S. Kweon. Accurate depth map estimation from a lenslet light field camera. In *The IEEE Conference on Computer Vision and Pattern Recognition (CVPR)*, June 2015.
- [21] N. K. Kalantari, T.-C. Wang, and R. Ramamoorthi. Learning-based view synthesis for light field cameras. *ACM Transactions on Graphics (TOG)*, 35(6):193, 2016.

- [22] D. Kingma and J. Ba. Adam: A method for stochastic optimization. Proceedings of the 3rd International Conference on Learning Representations (ICLR), 2015.
- [23] A. Krizhevsky, I. Sutskever, and G. E. Hinton. Imagenet classification with deep convolutional neural networks. In Advances in neural information processing systems, pages 1097–1105, 2012.
- [24] K. Kulkarni, S. Lohit, P. Turaga, R. Kerviche, and A. Ashok. Reconnet: Non-iterative reconstruction of images from compressively sensed random measurements. *IEEE Conference* on Computer Vision and Pattern Recognition (CVPR), 2016.
- [25] C. Ledig, L. Theis, F. Huszár, J. Caballero, A. Cunningham, A. Acosta, A. Aitken, A. Tejani, J. Totz, Z. Wang, et al. Photo-realistic single image super-resolution using a generative adversarial network. *IEEE Conference on Computer Vision and Pattern Recognition (CVPR)*, 2017.
- [26] M. Levoy and P. Hanrahan. Light field rendering. In Proceedings of the 23rd annual conference on Computer graphics and interactive techniques, pages 31–42. ACM, 1996.
- [27] J. Long, E. Shelhamer, and T. Darrell. Fully convolutional networks for semantic segmentation. In *Proceedings of the IEEE Conference on Computer Vision and Pattern Recognition*, pages 3431–3440, 2015.
- [28] J. Mairal, F. Bach, J. Ponce, and G. Sapiro. Online dictionary learning for sparse coding. In *Proceedings of the 26th annual* international conference on machine learning, pages 689– 696. ACM, 2009.
- [29] M. Mardani, E. Gong, J. Y. Cheng, S. Vasanawala, G. Zaharchuk, M. Alley, N. Thakur, S. Han, W. Dally, J. M. Pauly, et al. Deep generative adversarial networks for compressed sensing automates mri. arXiv preprint arXiv:1706.00051, 2017.
- [30] K. Marwah, G. Wetzstein, Y. Bando, and R. Raskar. Compressive light field photography using overcomplete dictionaries and optimized projections. ACM Transactions on Graphics (TOG), 32(4):46, 2013.
- [31] D. Mendlovic, R. Schleyen, and U. MENDLOVIC. System and method for light-field lmaging, July 13 2017. US Patent App. 15/321,505.
- [32] R. Ng, M. Levoy, M. Brédif, G. Duval, M. Horowitz, and P. Hanrahan. Light field photography with a handheld plenoptic camera. *Computer Science Technical Report CSTR*, 2(11):1–11, 2005.
- [33] Y. C. Pati, R. Rezaiifar, and P. S. Krishnaprasad. Orthogonal matching pursuit: Recursive function approximation with applications to wavelet decomposition. In Signals, Systems and Computers, 1993. 1993 Conference Record of The Twenty-Seventh Asilomar Conference on, pages 40–44. IEEE, 1993.
- [34] S. F. Ray. Applied photographic optics: Lenses and optical systems for photography, film, video, electronic and digital imaging. Focal Press, 2002.
- [35] T. Remez, O. Litany, R. Giryes, and A. M. Bronstein. Deep class-aware image denoising. In *IEEE International Confer*ence on *Image Processing (ICIP)*, 2017.
- [36] P. Sprechmann, A. M. Bronstein, and G. Sapiro. Learning efficient sparse and low rank models. *IEEE transactions on*

- pattern analysis and machine intelligence, 37(9):1821–1833, 2015.
- [37] P. P. Srinivasan, T. Wang, A. Sreelal, R. Ramamoorthi, and R. Ng. Learning to synthesize a 4d rgbd light field from a single image. *International Conference on Computer Vision* (ICCV), 2017.
- [38] Stanford. Stanford lytro light field archive. http://lightfields.stanford.edu/.
- [39] C. Szegedy, W. Liu, Y. Jia, P. Sermanet, S. Reed, D. Anguelov, D. Erhan, V. Vanhoucke, and A. Rabinovich. Going deeper with convolutions. In *Proceedings of the IEEE conference on computer vision and pattern recognition*, pages 1–9, 2015.
- [40] A. Veeraraghavan, R. Raskar, A. Agrawal, A. Mohan, and J. Tumblin. Dappled photography: Mask enhanced cameras for heterodyned light fields and coded aperture refocusing. *ACM Trans. Graph.*, 26(3):69, 2007.
- [41] G. Wetzstein, I. Ihrke, and W. Heidrich. On plenoptic multiplexing and reconstruction. *International journal of computer vision*, 101(2):384–400, 2013.
- [42] B. Wilburn, N. Joshi, V. Vaish, E.-V. Talvala, E. Antunez, A. Barth, A. Adams, M. Horowitz, and M. Levoy. High performance imaging using large camera arrays. In ACM Transactions on Graphics (TOG), volume 24, pages 765– 776. ACM, 2005.
- [43] F. Yu and V. Koltun. Multi-scale context aggregation by dilated convolutions. *Proceedings of the International Conference on Learning Representations (ICLR)*, 2016.
- [44] M. D. Zeiler, D. Krishnan, G. W. Taylor, and R. Fergus. Deconvolutional networks. In *IEEE Conference on Computer Vision and Pattern Recognition (CVPR)*, pages 2528–2535, 2010.
- [45] H. Zhao, O. Gallo, I. Frosio, and J. Kautz. Loss functions for image restoration with neural networks. *IEEE Transactions on Computational Imaging*, 3(1):47–57, 2017.

# **Appendices**

# A. Additional light field reconstruction examples

Here we present more results from our test set and other light field images from Stanford Lytro archive [38], which are not included in either the training or test set. In general, the images are taken from Stanford Lytro dataset [38] and the Lytro dataset provided by Kalantari et al. [21]. We present results for the noiseless and noisy cases. Each example includes our full light field image reconstruction and a close-up of the mark area from the four corner viewpoints of the reconstruction of each of the following methods: OMP, ADMM and ours. In each example, we marked an area with a significant disparity in the original light field image. Note that besides the noise and low-quality resolution in the sparsity-based reconstruction, there is also a loss of the angular resolution. It can be well observed in the OMP recovery of the White flower and Seahorse images in the noisy case (Figs. 13 and 14). OMP recovery loses the difference between the angles. Notice that in the noisy case, all techniques including ours encounter hardships in the color restoration. Due to high compression ratio, the noise causes errors in the color fidelity of the reconstructed light field (see Fig. 15). Nevertheless, our reconstruction still has high spatial and angular resolution in this case, which can be used for depth estimation (see Fig. 16), which is quite good. Also, it still outperforms the sparsity-based methods, which provide poor recovery.

We also we present here the three images that we made comparison with from Gupta et al. work [15] in the main paper: Seahorse, White flower and Purple flower (Fig. 9, 13 and 14). Since Gupta et al. did not provide any code, we cannot present their results but according to their reports, the average PSNR of the three images is 30.9 while ours is 31.56 in the noiseless case. Note that their network does not deal with color compression but decompress each channel separately. Therefore, our compression ratio is three times lower than theirs. They also use ASP [17], which creates a different  $\Phi$  compared to the coded mask approach we use.

## A.1. Noiseless case examples

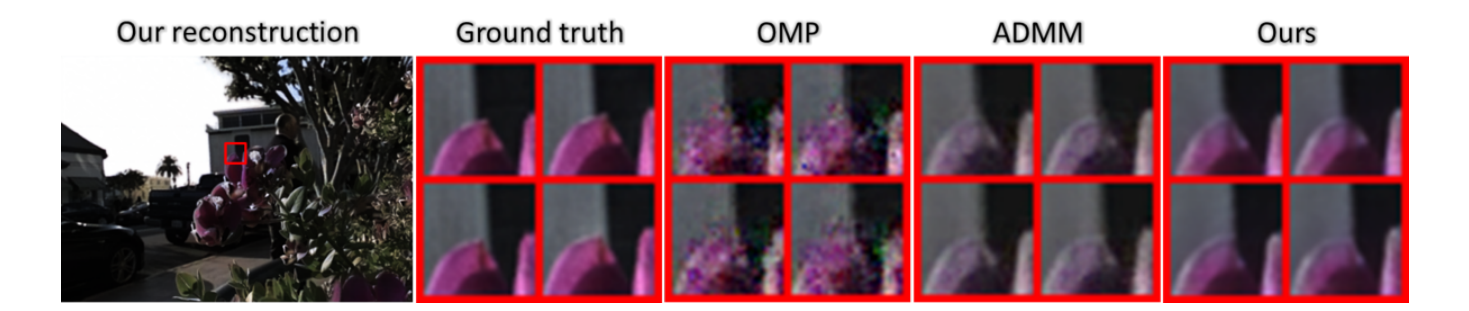


Figure 9: Purple flower

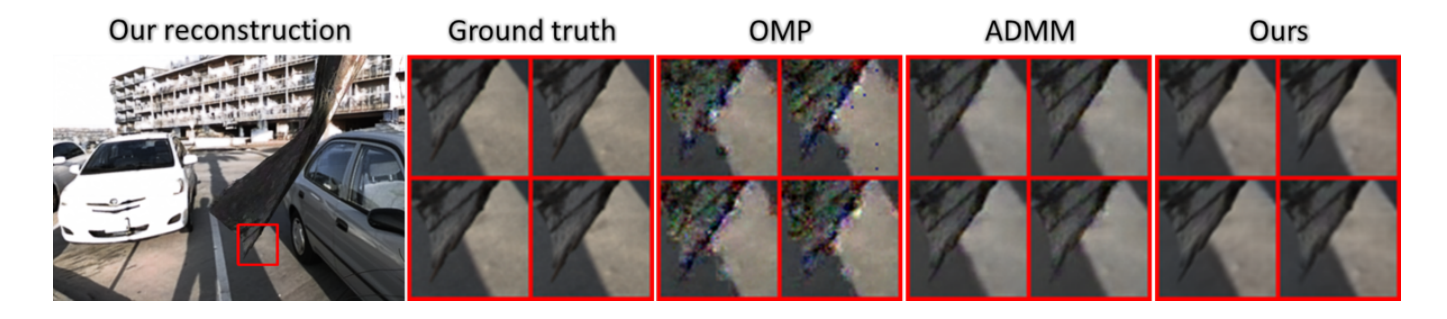


Figure 10: Cars

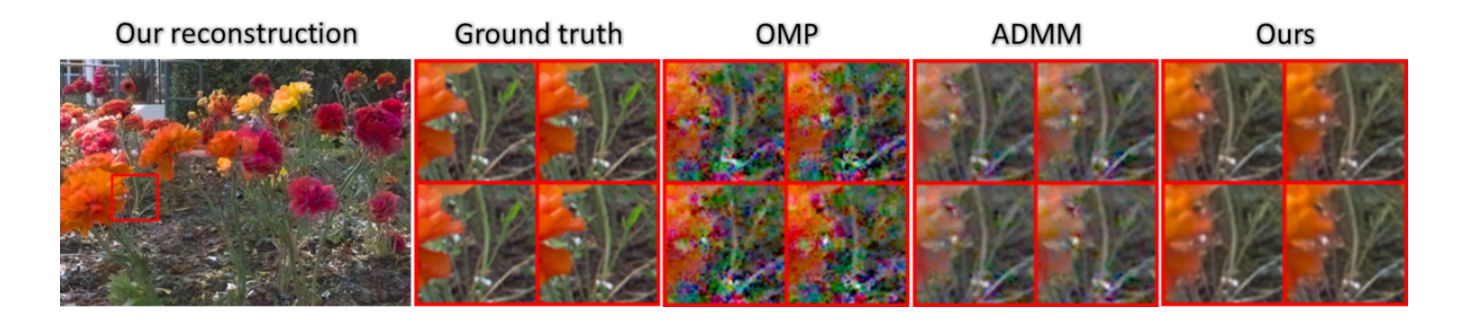


Figure 11: Garden

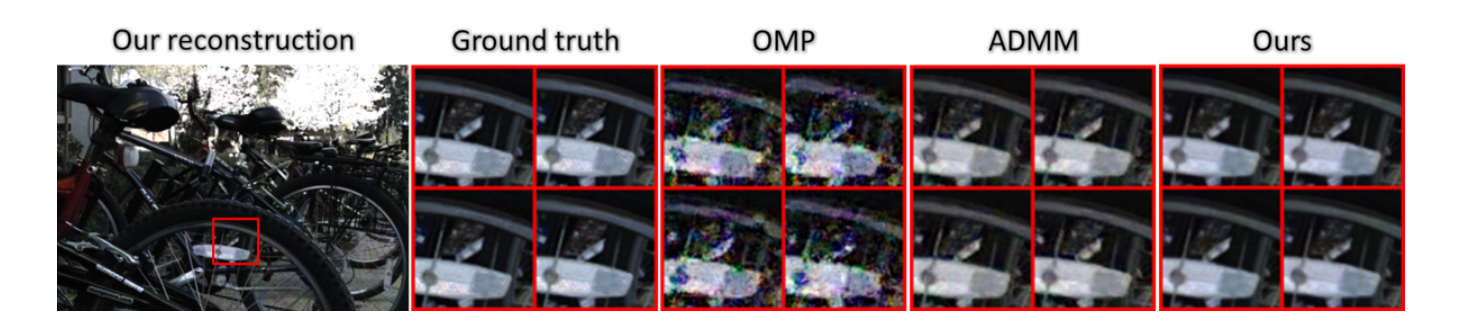


Figure 12: Bicycles

# A.2. Noisy case examples

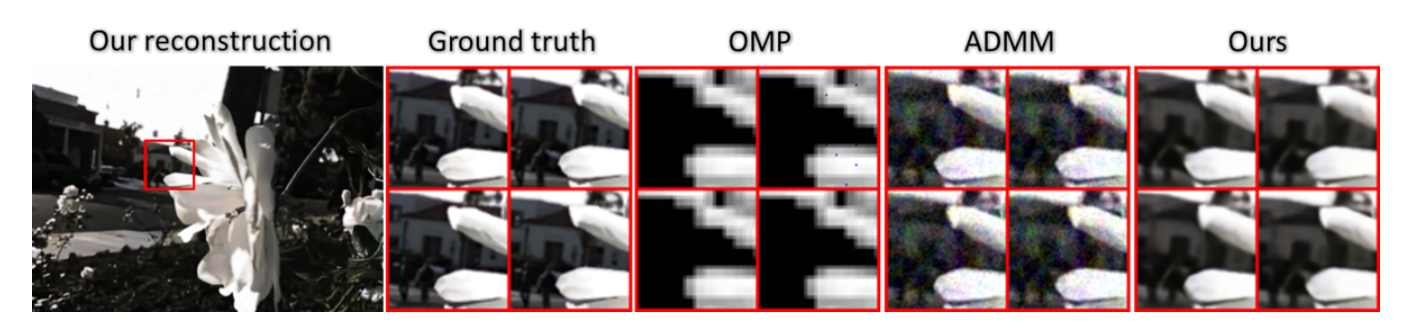


Figure 13: White flower

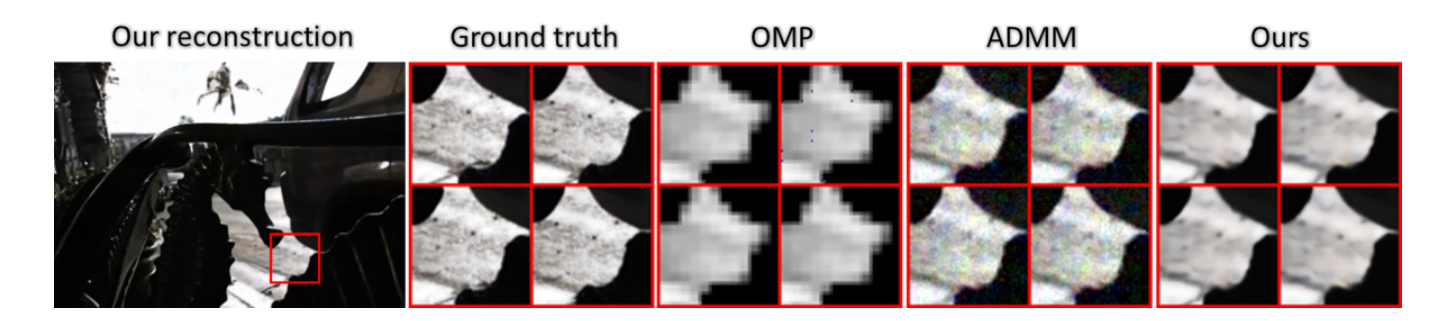


Figure 14: Seahorse

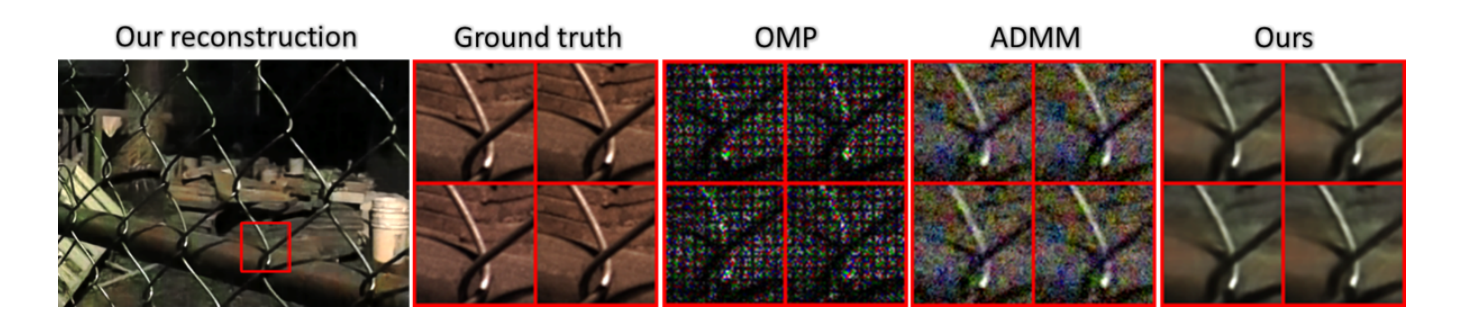


Figure 15: Fence

# B. Additional depth estimation examples

We present additional disparity map estimations images from the last section that do not appear in the main paper. For every light field scene we present (i) the ground truth image; (ii) Jeon at el. [20]; (iii) our network disparity map from the ground truth light field; and (iv) our network disparity map from the estimated light field calculated by our light field reconstruction network (noiseless case). Note that our network provides more accurate disparity maps compared to [20] when using the ground truth light field. When using the reconstructed one, the disparity maps from the compressed light field suffer from some blur and artifacts, both in spatial and angular dimensions due to estimation errors at the reconstructed light field, (as can be seen in Figs 9-15). Yet, this disparity estimation is quite accurate and competitive with the one achieved by [20].

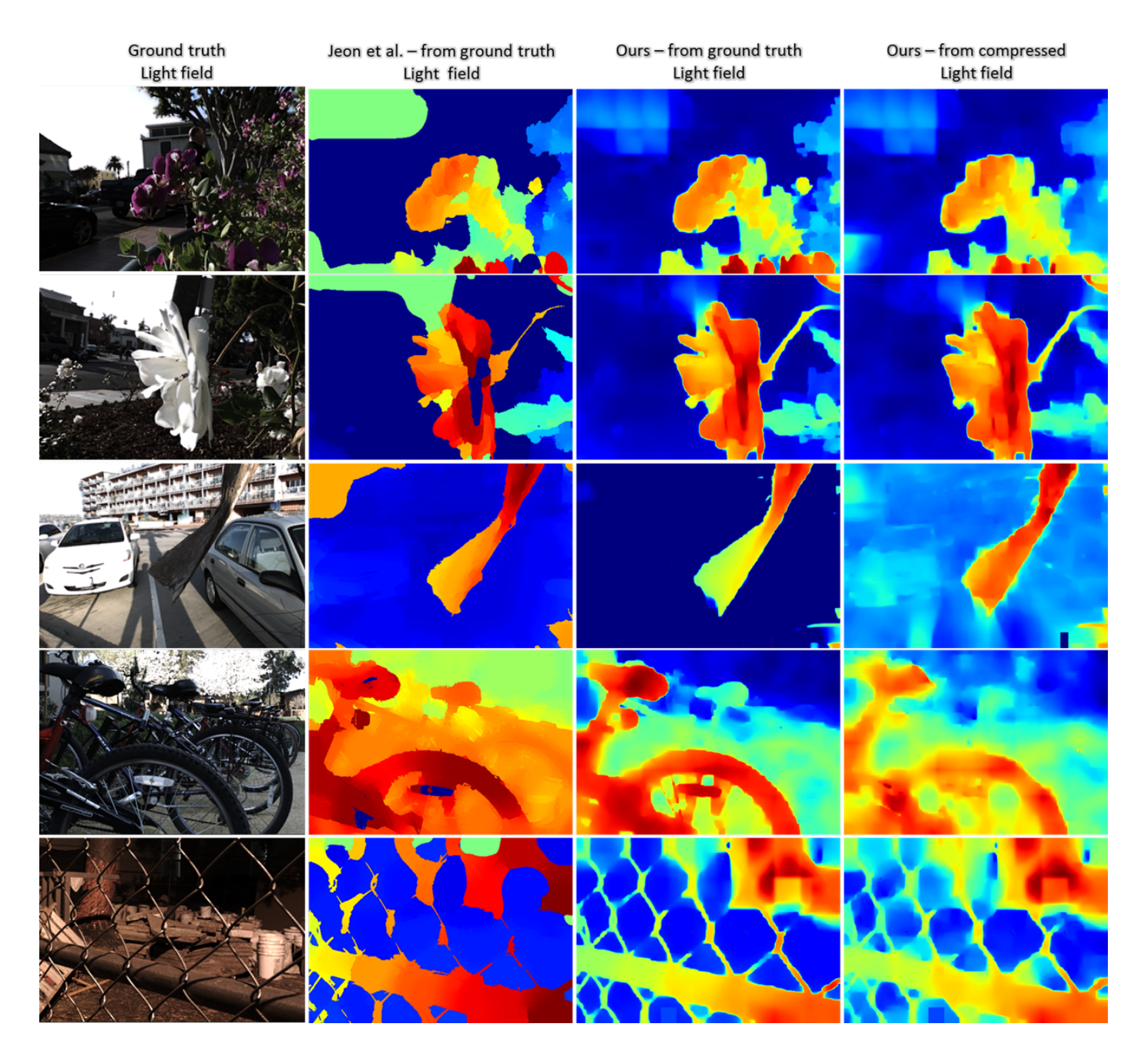


Figure 16: Additional depth estimation examples. We compare the results of Jeon et al. method [20] with our network for the ground truth light field. Also, we present our network disparity estimation from the reconstructed light field using our reconstruction network.